Theor Chem Acc (2007) 118:315–323
DOI 10.1007/s00214-007-0260-3

REGULAR ARTICLE

On the kinetic mechanism of reactions of hydroxyl radical with $CHF_2CH_{3-n}F_n$ ($n = 1$–3)

Yue-meng Ji · Ze-sheng Li · Jing-yao Liu

Received: 26 July 2006 / Accepted: 5 January 2007 / Published online: 23 February 2007

Abstract The potential energy surfaces of the reactions $CHF_2CH_{3-n}F_n$ ($n = 1$–3) + OH were investigated by MPWB1K and BMC-CCSD (single-point) methods. Furthermore, with the aid of canonical variational transition state theory including the small-curvature tunneling correction, the rate constants of the title reactions were calculated over a wide temperature range of 220–1,500 K. Agreement between the CVT/SCT rate constants and the experimental values is good. Our results show that the order of rate constants is $CHF_2CH_2F + OH > CHF_2CHF_2 + OH > CHF_2CF_3 + OH$. For reaction CHF_2CH_2F + OH, the 1-H-abstraction channel dominates the reaction at the whole temperature, while 2-H-abstraction channel appears to be competitive with the increase of temperature.

1 Introduction

Hydroflurocarbons (HFCs) have been widely studied because of the necessity of replacing chlorofluorocarbons (CFCs) in industrial applications [1–4]. Owing to their containing at least one C–H bond, HFCs are readily attacked by hydroxyl radical (OH). Thus, reactions of HFCs present in the troposphere with OH radical are believed to be important in determining their tropospheric lifetime, and hence influence the possible depletion of stratospheric ozone [6].

Y.-m. Ji · Z.-s. Li (✉) · J.-y. Liu
Institute of Theoretical Chemistry,
State Key Laboratory of Theoretical and Computational Chemistry, Jilin University, Changchun,
Jilin 130023, People's Republic of China
e-mail: zeshengli@mail.jlu.edu.cn

The present work concerns the reactions of OH radical with fluoroethanes $CHF_2CH_{3-n}F_n$ ($n = 1$–3) which have been studied experimentally by different groups [5–9]. In 1979, Clyne et al. [6] primarily measured the total rate constants for $CHF_2CH_2F + OH \rightarrow CF_2CH_2F/CHF_2CHF + H_2O$ (R1), $CHF_2CHF_2 + OH \rightarrow CHF_2CF_2 + H_2O$ (R2) and $CHF_2CF_3 + OH \rightarrow CF_2CF_3 + H_2O$ (R3) at 293–441, 294–434 and 293–441 K. For CHF_2CH_2F + OH (R1), the total rate constants measured by Barry et al. [5] [$(1.61 \pm 0.05) \times 10^{-14}$ cm^{-3} molecule^{-1} s^{-1}] and Martin et al. [7] [$(1.83 \pm 0.2) \times 10^{-14}$ cm^{-3} molecule^{-1} s^{-1}] are consistent with each other, while slight lower than Clyne et al. [6] [$(4.9 \pm 0.5) \times 10^{-14}$ cm^{-3} molecule^{-1} s^{-1}] at 298 K. The Arrhenius expression was obtained to be $k_1 = 2.65 \times 10^{-12}$ exp $[(-1542 \pm 500)/T]$ cm^{-3} molecule^{-1} s^{-1} by Barry et al. [5] in the temperature range 278–323 K. For CHF_2CHF_2 + OH (R2), Demore et al. [8] gave the Arrhenius expression as $k_2 = 1.6 \times 10^{-12}$ exp $(-1680/T)$ cm^{-3} molecule^{-1} s^{-1}, and the rate constant (5.7×10^{-15} cm^{-3} molecule^{-1} s^{-1}) agrees well with the value given by Clyne et al. [6] [$(6.9 \pm 1.9) \times 10^{-15}$ cm^{-3} molecule^{-1} s^{-1}] at 298 K. In 1991, Talukdar et al. [9] obtained the Arrhenius expression of $(5.41 \pm 0.83) \times 10^{-13}$ exp $[(-1,700 \pm 100)/T]$ cm^{-3} molecule^{-1} s^{-1} for R3. Experimentally, the reactions of OH radical with $CHF_2CH_{3-n}F_n$ ($n = 1$–3) were studied mainly below 441 K, and the branching ratio of CHF_2CH_2F + OH has not been reported. Thus, to gain a deeper insight into the reaction mechanisms and branching ratio of R1 at a wide temperature range, further theoretical studies are very desirable. The theoretical reaction enthalpies and classical barriers of the title reactions have been estimated by Martell and co-workers [10], but to the best of our knowledge the theoretical rate constants

for the title reactions have not yet been studied theoretically.

Here, a dual-level (X//Y) direct dynamics method [11–13] is applied to study the kinetics of these reactions over a wide temperature range and the comparison between theoretical and experimental results is discussed. By means of the POlYRATE 9.1 program [20], the rate constants are calculated using the variational transition-state theory (VTST) [14–16] developed by Truhlar and co-workers.

2 Calculation methods

All the electronic structure calculations were carried out with the GAUSSIAN03 program [17]. The equilibrium geometries and frequencies of the stationary points involved in these reactions were calculated at two levels, i.e., modified Perdew–Wang and Becke's 1995 correlation 1-parameter model for kinetics (MPWB1K) and the restricted or unrestricted second-order Møller–Plesset perturbation theory (MP2), using the 6-311+G(d,p) basis set. The zero-point energy (ZPE) contributions (scaled by a factor of 0.95) were obtained at the MPWB1K level. The minimum-energy path (MEP) was constructed with the intrinsic reaction coordinate (IRC) theory with a gradient step size of 0.01 $(\text{amu})^{1/2}$ bohr at the same level to confirm that the transition state really connects with minima along the reaction path. To yield more accurate energetic information, single-point energy calculations of each reaction channel were performed at the BMC-CCSD [18] level (a new multi-coefficient correlation method based on coupled cluster theory with single and double excitations (CCSD) proposed by Lynch and Truhlar) using the MPWB1K optimized geometries. Also, we used the same geometries for coupled cluster approach with single and double substitutions including a perturbative estimate of connected triples substitutions with the 6-311+G(3df,2p) basis set (CCSD(T)/6-311+G(3df,2p)). The dual-level potential profile along the reaction path is further refined with the interpolated single-point energy (ISPE) method [19], in which a few extra single-point calculations are needed to correct the lower level reaction path.

By means of POLYRATE 9.1 program [20], the theoretical rate constants were calculated by canonical variational transition state theory (CVT) [21] with the small-curvature tunneling correction (SCT) [22,23] proposed by Truhlar and co-workers. The CVT [21] rate constant can be obtained by variationally minimizing the generalized transition-state theory rate constant $k^{\mathrm{GT}}(T,s)$ with respect to the dividing surface at s, that is,

$$k^{\mathrm{CVT}}(T) = \min_{s} k^{\mathrm{GT}}(T,s)$$

where

$$k^{\mathrm{GT}}(T,s) = \frac{\sigma}{h\beta}\frac{Q^{\mathrm{GT}}(t,s)}{Q^{R}(T)}\exp\left[-\beta V_{\mathrm{MEP}}(s)\right]$$

In these equations, s is the location of the generalized transition state on IRC; σ is the symmetry factor accounting for the possibility of two or more symmetry-related reaction paths; β equals $(k_B T)^{-1}$ where k_{B} is Boltzmann's constant, h is Planck's constant; $Q^{\mathrm{R}}(T)$ is the reactant's partition function per unit volume, excluding symmetry numbers for rotation; $V_{\mathrm{MEP}}(s)$ is the classical energy along the MEP overall zero of energy at the reactants; $Q^{\mathrm{GT}}(T,s)$ is the partition function of generalized transition state at s with the local zero of energy at $V_{\mathrm{MEP}}(s)$ and with all rotational symmetry numbers set to unity. To include the tunneling effect, the CVT rate constant is multiplied by a transmission coefficient computed with the small-curvature tunneling (SCT) [22,23] approximation, which is denoted by $k^{\mathrm{CVT/SCT}}(T)$. For the SCT calculations, the effective reduced mass is obtained by a sixth-order Lagrangian interpolation. The Euler single-step integrator with a step size of 0.0005 $(\text{amu})^{1/2}$ bohr is used to follow the MEP. The generalized normal-mode analysis is performed for each 0.05 $(\text{amu})^{1/2}$ bohr. In the calculation of the electronic partition functions, the two electronic states for the OH radical, with a 140 cm^{-1} splitting in the $^2\Pi$ ground state, were considered. The curvature components were calculated using a quadratic fit to obtain the derivative of the gradient with respect to the reaction coordinate.

3 Results and discussion

3.1 Electronic structure calculations

The optimized geometries of all the reactants, products, and transition states optimized at the MPWB1K/6-311+G(d,p) and MP2/6-311+G(d,p) levels along with the available experimental values [24–26] are shown in Fig. 1. When a comparison is possible, the geometries of all the stationary points obtained at the MPWB1K and MP2 levels are both in reasonable agreement with the corresponding experimental values. As CHF_2CH_2F is an asymmetrical molecule, the hydrogen atoms in CHF_2CH_2F are not equivalent and can be classified into three categories. Thus, the reaction CHF_2CH_2F + OH will pass through three transition states leading to two products CF_2CH_2F and CHF_2CHF, i.e., Path I (1-H-abstraction): R1 → TS1a → CF_2CH_2F; Path II

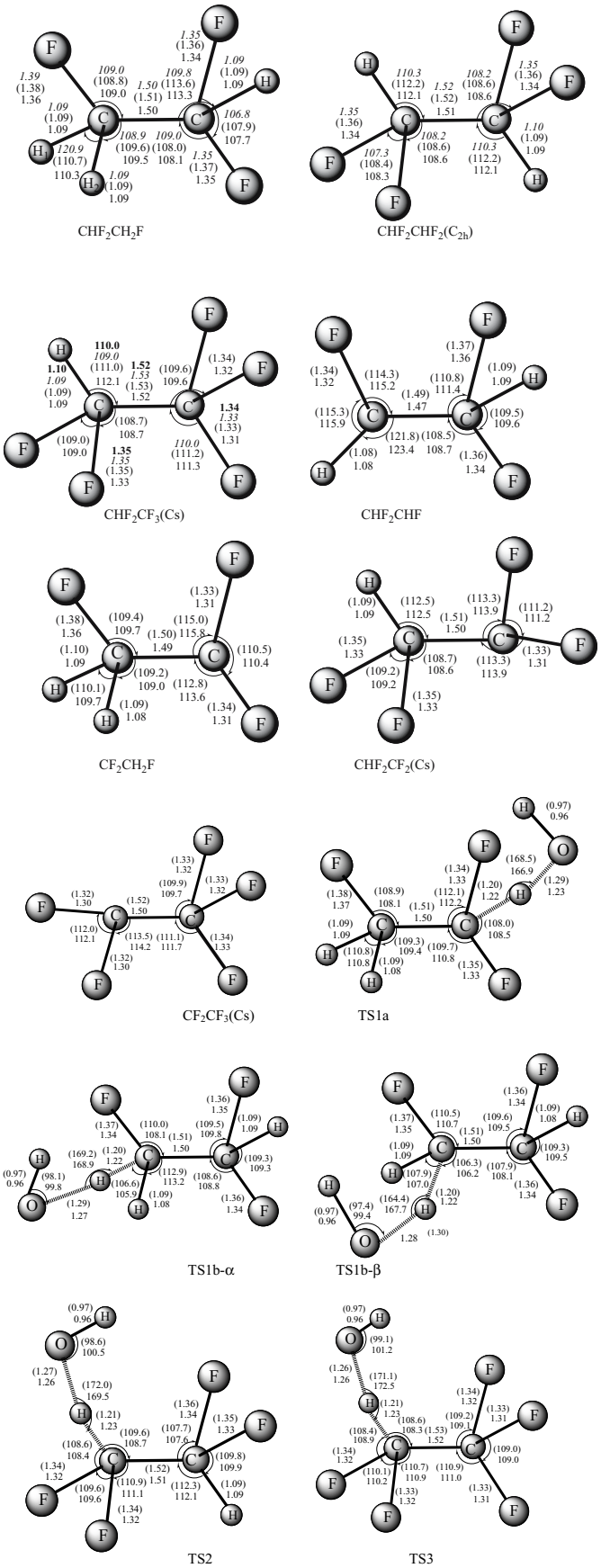

Fig. 1 Equilibrium geometries of reactants, products, and transition states at the MPWB1K/6-311+G(d,p) level. The values in parentheses are optimized at the MP2/6-311+G(d,p) level; the values in the *italic type* and *boldface* are the experimental values [24–26], respectively. Bond lengths are in angstroms, and angles are in degrees

Table 1 Calculated and available experimental frequencies (cm^{-1}) of the stationary points at the MPWB1K/6-311+G(d,p) level

Species	MPWB1K/6-311+G(d,p)
CHF_2CH_2F	116(115)[a], 245(237)[a], 439(416)[a], 485(469)[a], 598(564)[a], 939(903)[a], 1143(1090)[a], 1166(1120)[a], 1174(1133)[a], 1210(1163)[a], 1301(1248)[a], 1372(1343)[a], 1434(1413)[a], 1502(1468)[a], 1522(1498)[a], 3147(2947)[a], 3182(2995)[a], 3215(3010)[a]
CHF_2CHF_2	81(82)[a], 201(204)[a], 368(362)[a], 415(413)[a], 500(480)[a], 562(542)[a], 650(625)[a], 1148(1081)[a], 1180(1106)[a], 1191(1125)[a], 1204(1136)[a], 1216(1149)[a], 1351(1320)[a], 1388(1335)[a], 1417(1365)[a], 1520(1442)[a], 3184(2995)[a], 3196(2995)[a]
CHF_2CF_3	67(82)[b], 203(216)[b], 241(246)[b], 368(361)[b], 428(413)[b], 538(508)[b], 599(523)[b], 604(577)[b], 752(725)[b], 905(867)[b], 1197(1111)[b], 1216(1145)[b], 1256(1198)[b], 1292(1218)[b], 1366(1309)[b], 1411(1359)[b], 1502(1393)[b], 3192(3008)[b]
CF_2CH_2F	89, 244, 445, 452, 606, 928, 1060, 1159, 1265, 1306, 1361, 1475, 1513, 3098, 3197
CHF_2CHF	81, 246, 408, 450, 570, 650, 1083, 1147, 1179, 1255, 1332, 1394, 1520, 3178, 3292
CHF_2CF_2	63, 198, 364, 399, 503, 566, 667, 1016, 1195, 1214, 1307, 1334, 1407, 1487, 3126
CF_2CF_3	55, 202, 221, 372, 433, 532, 607, 632, 727, 861, 1182, 1258, 1306, 1367, 1483
TS1a	1451*i*, 88, 105, 134, 234, 263, 439, 448, 501, 667, 852, 947, 1130, 1152, 1208, 1249, 1285, 1342, 1442, 1506, 1518, 3145, 3220, 3884
TS1b-α	1492*i*, 66, 92, 152, 217, 245, 438, 487, 598, 722, 829, 960, 1138, 1170, 1193, 1203, 1224, 1352, 1418, 1462, 1474, 3166, 3195, 3895
TS1b-β	1439*i*, 62, 80, 142, 167, 255, 409, 461, 597, 697, 845, 945, 1152, 1172, 1190, 1206, 1298, 1326, 1402, 1453, 1509, 3188, 3199, 3898
TS2	1592*i*, 66, 87, 120, 180, 205, 369, 391, 481, 517, 593, 686, 844, 1130, 1170, 1184, 1219, 1279, 1287, 1400, 1447, 1493, 3174, 3886
TS3	1633*i*, 36, 58, 93, 131, 206, 247, 370, 418, 439, 560, 605, 622, 769, 814, 951, 1166, 1220, 1283, 1307, 1315, 1434, 1466, 3890

[a] From Ref. [28]
[b] From Ref. [29]

and III (2-H-abstraction): R1 → TS1b-α/TS1b-β → CHF_2CHF. At the MPWB1K level, for the transition state structures of TS1a, TS1b-α, and TS1b-β, the breaking bonds C–H are all elongated by 12% compared to the C–H equilibrium bond length in isolated CH_2FCHF_2; the forming bonds O–H are stretched by 29, 34, and 35%, respectively, with respect to the equilibrium bond length of the molecule H_2O. For TS2 and TS3, the case is similar; the breaking C–H bonds both increase by 13% and the formed bonds are both stretched by 33%. The elongation of the forming bonds is greater than that of the breaking bonds, indicating that the above five TSs are reactant-like, i.e., all these reactions proceed via "early" transition states. The similar character can also be concluded from the geometrical structures optimized at the MP2/6-311+G(d,p) level. This behavior is in keeping with Hammond's postulate, since all reactions are exothermic [27].

Table 1 lists the harmonic vibrational frequencies (unscaled) of all the stationary points computed at the MPWB1K level along with the available experimental values [28,29]. The calculated frequencies are in good agreement with the available experimental data at the MPWB1K level as shown in Table 1. The number of imaginary frequencies (0 or 1) indicates whether a minimum or a transition state has been located. The transition states in Table 1 are identified by normal-mode analysis to have one and only one imaginary frequency with the values of 1451 *i*(TS1a), 1492 *i*(TS1b-α), 1439 *i*(TS1b-β), 1592 *i*(TS2), and 1633 *i*(TS3), respectively.

The reaction enthalpies (ΔH^{o}_{298}) of the title reactions were calculated at three levels, i.e., MPWB1K/6-311+G(d,p), BMC-CCSD//MPWB1K and CCSD(T)/6-311+G(3df,2p)//MPWB1K. The corresponding results and the experimental data are listed in Table 2, in which the experimental results of -16.7 ± 5.7 kcal mol^{-1} (R1a), -15.2 ± 5.7 kcal mol^{-1}(R1b), -15.6 ± 6.6 kcal mol^{-1} (R2), and -15.7 ± 4.07 kcal mol^{-1} (R3) were derived from the knowledge of the standard heats of formation (CH_2FCHF_2 – 159.0 ± 2.0 kcal mol^{-1} [30]; CHF_2CHF_2 – 210.0 ± 1.0 kcal mol^{-1} [30]; CF_3CHF_2 – 264.0 ± 1.0 kcal mol^{-1} [30]; CH_2FCF_2 – 107.5 ± 3.6 kcal mol^{-1} [31]; $CHFCHF_2$ – 109.0 ± 3.6 kcal mol^{-1} [31]; CF_2CHF_2 – 158.9 ± 4.5 kcal mol^{-1} [31]; CF_3CHF_2 – 213.0 ± 2.0 kcal mol^{-1} [30]; H_2O – 57.8 kcal mol^{-1} [32]; OH 8.91 ± 0.07 kcal mol^{-1} [33]). From Table 2, it is known that the calculated results for the reaction enthalpies obtained at the CCSD(T)/6-311+G(3df,2p) level are obviously less negative than the corresponding BMC-CCSD//MPWB1K results, and the better agreement between theory and experiment is obtained at the BMC-CCSD//MPWB1K level. Thus, in this investigation, the BMC-CCSD method is adopted to refine the energies along the MEP as well as the potential energy barriers, and the results at the BMC-CCSD//MPWB1K/6-311+G(d,p) level are employed to study the rate constants.

Table 2 Enthalpies (in kcal mol^{-1}) at various levels and available experimental values

levels	$CH_2FCHF_2 + OH \rightarrow CH_2FCF_2 + H_2O$	$CH_2FCHF_2 + OH \rightarrow CHFCHF_2 + H_2O$	$CHF_2CHF_2 + OH \rightarrow CF_2CHF_2 + H_2O$	$CF_3CHF_2 + OH \rightarrow CF_3CF_2 + H_2O$
MPWB1K/6-311+G(d,p)	– 13.65	– 14.45	– 12.41	– 12.57
BMC-CCSD//MPWB1K	– 17.40	– 18.64	– 16.18	– 16.27
CCSD(T)//MPWB1K	– 14.63	– 15.59	– 13.41	– 13.42
Exptl.[a]	-16.7 ± 5.7	-15.2 ± 5.7	-15.6 ± 6.6	-15.7 ± 4.1

[a] From Refs. [30–33]

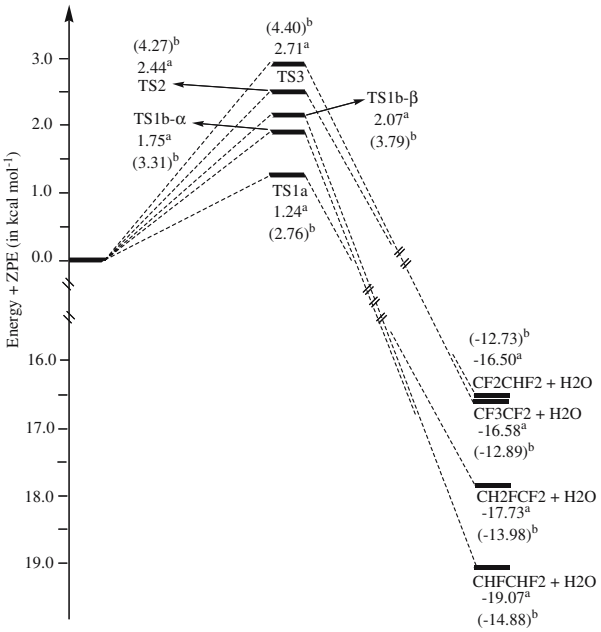

[a]Calculted at the BMC-CCSD//MPWB1K/6-311+G(d,p) level

[b]Calculted at the MPWB1K/6-311+G(d,p) level

Fig. 2 Schematic pathways for the reactions R1-R3

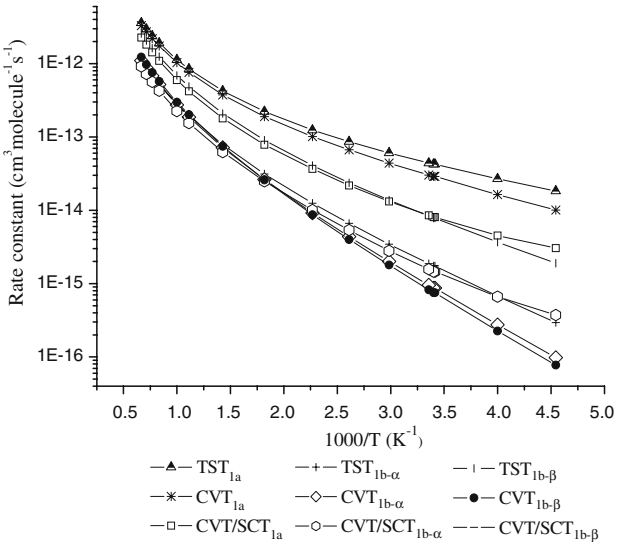

Fig. 3 Plots of the TST, CVT, and CVT/SCT rate constants calculated at the BMC-CCSD//MPWB1K/6-311+G(d,p) level versus $1000/T$ between 220 and 1,500 K for $CH_2FCHF_2 + OH \rightarrow CH_2FCF_2 + H_2O$, $CH_2FCHF_2 + OH \xrightarrow{TS1b-\alpha} CHFCHF_2 + H_2O$, and $CH_2FCHF_2 + OH \xrightarrow{TS1b-\beta} CHFCHF_2 + H_2O$

Figure 2 shows a schematic potential energy surface of each reaction with zero point energy (ZPE) corrections, and the energy of reactant R is set zero for reference. The potential barrier heights with ZPE correction are 2.76, 3.31, and 3.79 kcal mol^{-1} for R1a, R1b-α, and R1b-β, respectively, at the MPWB1K level, while they all decreased by about 1.5 kcal mol^{-1} at the BMC-CCSD level. Even at the BMC-CCSD level the barrier heights of R1a taking the value of 0.6–1.0 kcal mol^{-1} is lower than that of other channels, indicating that 1-H-abstraction channel is more favorable than 2-H-abstraction channel. For the reactions CHF_2CHF_2 + OH (R2) and CF_3CHF_2 + OH (R3), the potential barrier heights with ZPE correction are 4.27 and 4.40 kcal mol^{-1} at the MPWB1K level, while at the BMC-CCSD//MPWB1K level, the corresponding values are 2.44 and 2.71 kcal mol^{-1}, respectively.

4 Rate constants calculation

Dual-level (X//Y) direct dynamics calculations are carried out for R1a and R2a using the variational transition-state theory (VTST) [13–15] approach. The PES information of each reaction obtained at the BMC-CCSD//MPW1K/6-311+G(d,p) level is put into the POLYRATE 9.1 [18] program to calculate the VTST rate constants over the temperature range from 220 to 1,500 K.

The TST, CVT, and CVT/SCT rate constants for R1a, R1b-α and R1b-β are presented in Fig. 2. Figure 2 shows that the variational effect is important for R1a and R1b-α at lower temperatures and becomes less important in the high temperature range. For R1b-β, the ratios of k(CVT)/k(TST) are 0.04, 0.29, and 0.48 at 220, 550, and 1,500 K, respectively, and this indicates that the variational effect is very large in the whole temperature range. By comparing the results between CVT and CVT/SCT,

Table 3 Calculated CVT/SCT rate constants along with the experimental data for the reaction $CH_2FCHF_2 + OH$

T (K)	k_{1a}	$k_{1b-\alpha}$	$k_{1b-\beta}$	k_{1b}	k_1	Exptl.
220	3.04×10^{-15}	3.73×10^{-16}	3.53×10^{-16}	7.26×10^{-16}	3.77×10^{-15}	
250	4.52×10^{-15}	6.62×10^{-16}	6.10×10^{-16}	1.27×10^{-15}	5.79×10^{-15}	
293	7.98×10^{-15}	1.44×10^{-15}	1.32×10^{-15}	2.76×10^{-15}	1.07×10^{-14}	[c] $(4.98 \pm 0.82) \times 10^{-14}$
294	8.08×10^{-15}	1.46×10^{-15}	1.35×10^{-15}	2.81×10^{-15}	1.09×10^{-14}	[c] $(4.68 \pm 0.4) \times 10^{-14}$
298	8.49×10^{-15}	1.57×10^{-15}	1.44×10^{-15}	3.01×10^{-15}	1.15×10^{-14}	[a] $(1.61 \pm 0.05) \times 10^{-14}$ [b] $(1.83 \pm 0.2) \times 10^{-14}$ [c] $(4.90 \pm 0.5) \times 10^{-14}$
335	1.32×10^{-14}	2.80×10^{-15}	2.65×10^{-15}	5.45×10^{-15}	1.87×10^{-14}	[c] $(6.74 \pm 0.43) \times 10^{-14}$
383	2.18×10^{-14}	5.37×10^{-15}	5.24×10^{-15}	1.06×10^{-14}	3.24×10^{-14}	[c] $(9.09 \pm 0.42) \times 10^{-14}$
441	3.67×10^{-14}	1.01×10^{-14}	1.04×10^{-14}	2.05×10^{-14}	5.72×10^{-14}	[c] $(1.89 \pm 0.06) \times 10^{-13}$
550	7.85×10^{-14}	2.49×10^{-14}	2.85×10^{-14}	5.34×10^{-14}	1.32×10^{-13}	
700	1.79×10^{-13}	6.22×10^{-14}	7.61×10^{-14}	1.38×10^{-13}	3.17×10^{-13}	
900	4.19×10^{-13}	1.55×10^{-13}	1.96×10^{-13}	3.51×10^{-13}	7.70×10^{-13}	
1000	5.96×10^{-13}	2.25×10^{-13}	2.87×10^{-13}	5.12×10^{-13}	1.11×10^{-12}	
1200	1.09×10^{-12}	4.27×10^{-13}	5.46×10^{-13}	9.73×10^{-13}	2.06×10^{-12}	
1300	1.42×10^{-12}	5.63×10^{-13}	7.18×10^{-13}	1.28×10^{-12}	2.70×10^{-12}	
1400	1.81×10^{-12}	7.27×10^{-13}	9.24×10^{-13}	1.65×10^{-12}	3.46×10^{-12}	
1500	2.27×10^{-12}	9.20×10^{-13}	1.17×10^{-12}	2.09×10^{-12}	4.36×10^{-12}	

[a] From Ref. [5]
[b] From Ref. [7]
[c] From Ref. [6]

the SCT correction should be taken into account in the rate constant calculation for three channels of R1 at low temperature range as can be seen from Fig. 3. For R1, as represented in Fig. 3, we can find that the CVT rate constants are always larger than the CVT/SCT values and this may come from the quantum effect. As pointed out by Taghikhani and Parsafar [34] the quantum effect decreases the rate constant. This is an unusual case of dynamics calculation in which quantum effects preclude particles (supermolecules) to pass over the classical barrier. And this is a special case in which the nonclassical reflection effect, at energies above the barrier, overcomes the tunneling through the classically forbidden region of the barrier. This makes the CVT/SCT rate constants decrease.

The CVT/SCT rate constants k_{1a} and k_{1b} and the total rate constant k_1 along with the available experimental values are listed in Table 3. Theoretical rate constants are plotted against 1,000/T (K^{-1}) in Fig. 4a, and the temperature dependence of the k_{1a}/k_1 and k_{1b}/k_1 branching ratios is exhibited in Fig. 4b. It is found that the 1-H-abstraction leading to the product $CH_2FCF_2 + H_2O$ dominates the reaction at the whole temperature range, while the contribution of 2-H-abstraction becomes competitive at higher temperature. For example, the k_{1b}/k_1 ratios are 19% at 220 K, 40% at 550 K, and 48% at 1,500 K. It appears that the total CVT/SCT rate constants shown in Table 3 are in better agreement with reliable experimental data given by Barry et al. [5] and Martin et al. [7], while the calculated data is lower than the result obtained by Clyne et al. [6] at 298 K. Moreover, the Arrhenius expression of $k_1 = 7.11 \times 10^{-13} \exp(-1,226.9/T)\ \mathrm{cm^{-3}\ molecule^{-1}\ s^{-1}}$ fitted by the CVT/SCT rate constants in the temperature range 278–323 K is in good accord with that reported by Barry et al. [5] $k_1 = 2.65 \times 10^{-12} \exp[(-1,542 \pm 500)/T]\ \mathrm{cm^{-3}\ molecule^{-1}\ s^{-1}}$. The three-parameter expressions by fitting the CVT/SCT rate constants in range of 220–1500 K for three channels of R1 are obtained and expressed as $k_{1a} = 1.13 \times 10^{-22}\, T^{3.26} \exp(116.4/T)$, $k_{1b-\alpha} = 3.78 \times 10^{-22}\, T^{3.01} \exp(555.2/T)$, $k_{1b-\beta} = 1.41 \times 10^{-22}\, T^{3.18} \exp(568.4/T)$, and $k_{1b} = 4.40 \times 10^{-22}\, T^{3.10} \exp(560.1/T)\ \mathrm{cm^{-3}\ molecule^{-1}\ s^{-1}}$.

As shown from Fig. 5, in which the rate constants of TST, CVT, and CVT/SCT for CHF_2CHF_2 + OH (R2) are plotted, the large difference between the TST and CVT rate constants appears and this implies that the variational effect is important for this reaction as well. On the other hand, by comparing the results of the CVT and CVT/SCT, the SCT correction should be taken into account in the rate constant calculations for R2 at low temperature range, with the $k_{(CVT/SCT)}/k_{(CVT)}$ ratios of 2.40 at 220 K, and the same conclusion can be obtained for R3. The CVT/SCT rate constants of R2 and R3 along with the available experimental values [6–9] are listed in Table 4. For R2, our calculated rate constants are consistent with the experimental ones with the largest deviation within a factor of 2.5. In the temperature range

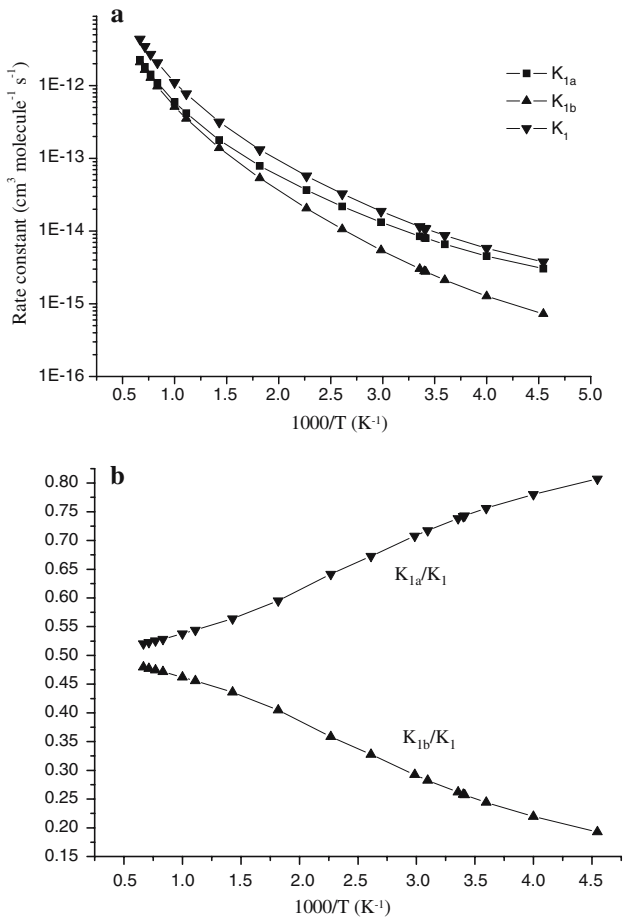

Fig. 4 **a** Plot of the calculated individual rate constants k_{1a} and k_{1b}, and the total rate constants k_1 versus $1000/T$ between 220 and 1,500 K. **b** Calculated branching ratio versus $1000/T$ between 220 and 1,500 K

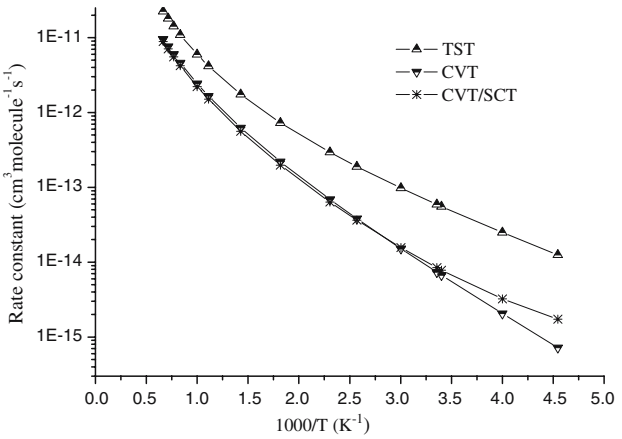

Fig. 5 Plots of the TST, CVT, and CVT/SCT rate constants calculated at the BMC-CCSD//MPWB1K/6-311+G(d,p) level versus $1000/T$ between 220 and 1,500 K for $CHF_2CHF_2 + OH \rightarrow CHF_2CF_2 + H_2O$

298–358 K, the Arrhenius expression fitted by the CVT/SCT results is $k_2 = 3.63 \times 10^{-12} \exp(-1,808/T)$ $cm^{-3}molecule^{-1}\,s^{-1}$, and is in good agreement with that given by Demore et al. [8], $k_2 = 1.6 \times 10^{-12} \exp(-1,680/T)$ $cm^{-3}\,molecule^{-1}\,s^{-1}$. Similar to reaction R2, the fitted two-parameter expression from the CVT/SCT rate constants for R3 in 220–360 K is $k_3 = 5.46 \times 10^{-12} \exp(-2,187/T)\,cm^{-3}\,molecule^{-1}\,s^{-1}$, in line with the experimental expression of $k_3 = (5.41 \pm 0.83) \times 10^{-13} \exp[(-1,700 \pm 100)/T]\,cm^{-3}\,molecule^{-1}\,s^{-1}$ given by Talukdar et al. [9]. The theoretical rate constants decrease in the order of $k_1 > k_2 > k_3$, thus, the reactivity decreases with fluorine substitution increase at the CH_2F group position of fluoroethane.

The activation energies (E_a) obtained from the CVT/SCT results by several two-parameter expression fits along with the available experimental values [5,6,8,9] are listed in Table 5. The theoretical results of E_a for the reactions CH_2FCHF_2 + OH (R1) and CHF_2CHF_2 + OH (R2) are in good agreement with the experimental ones for the considered temperature regions. For the CF_3CHF_2 + OH reaction, our calculated E_a deduced from the CVT/SCT rate constants are closer to that of Talukdar and co-workers [9], in the measured temperature range 220–360. Also, the discrepancy of E_a between our calculated values and that of Clyne and co-workers [6] is about 2.1 ± 0.2 kcal mol^{-1}. The good agreement between theoretical and experimental rate constants and between theoretical and experimental activation energies indicates that the present calculations can provide reliable predictions of the rate constants for the title reactions at higher temperatures, which will be useful for the atmospheric modeling calculations.

Finally, to provide estimate for the rates of the reactions in higher temperatures where no experimental values are available, three-parameter fits were made for the title reactions over the range 220–1,500 K; these fits give the following expressions (in cm^{-3} $molecule^{-1}$ s^{-1}):

$$k_1 = 1.61 \times 10^{-22}\, T^{3.31} \exp(215.6/T),$$
$$k_2 = 3.27 \times 10^{-21}\, T^{3.05} \exp(747.3/T),$$
$$k_3 = 3.21 \times 10^{-22}\, T^{3.42} \exp(955.8/T).$$

5 Conclusion

In this paper, we employ density functional theory to study three hydrogen abstraction reactions of $CHF_2CH_{3-n}F_n$ (n = 1–3) with OH radical. The potential energy surface information is obtained at the MPWB1K/6-311+G(d, p) level and the energies of the stationary points are corrected at the BMC-CCSD level. The rate constants are calculated using variational transition

Table 4 Calculated CVT/SCT rate constants with the experimental data for the reactions $CHF_2CHF_2 + OH$ and $CF_3CHF_2 + OH$

T (K)	$CHF_2CHF_2 + OH \rightarrow CF_2CHF_2 + H_2O$		T(K)	$CF_3CHF_2 + OH \rightarrow CF_3CF_2 + H_2O$	
	CVT/SCT	Exptl.		CVT/SCT	Exptl.
220	1.73×10^{-15}		220	4.54×10^{-16}	
250	3.22×10^{-15}		293	3.20×10^{-15}	[b] $(5.0 \pm 2.2) \times 10^{-15}$
294	7.82×10^{-15}	[b] $(5.3 \pm 1.5) \times 10^{-15}$	294	3.27×10^{-15}	[b] $(4.90 \pm 0.05) \times 10^{-15}$
298	8.43×10^{-15}	[a] 5.70×10^{-15} [b] $(6.90 \pm 1.9) \times 10^{-15}$	298	3.57×10^{-15}	[c] $(2.49 \pm 0.05) \times 10^{-15}$ [b] $(5.0 \pm 1.0) \times 10^{-15}$
333	1.57×10^{-14}	[b] $(1.88 \pm 0.27) \times 10^{-14}$	336	7.67×10^{-15}	[b] $(6.20 \pm 1.8) \times 10^{-15}$
389	3.63×10^{-14}	[b] $(2.12 \pm 0.41) \times 10^{-14}$	378	1.6×10^{-14}	[b] $(1.13 \pm 0.33) \times 10^{-14}$
434	6.38×10^{-14}	[b] $(4.82 \pm 0.36) \times 10^{-14}$	441	4.03×10^{-14}	[b] $(1.58 \pm 0.29) \times 10^{-14}$
550	1.98×10^{-13}		550	1.36×10^{-13}	
700	5.62×10^{-13}		700	4.57×10^{-13}	
900	1.51×10^{-12}		900	1.45×10^{-12}	
1000	2.22×10^{-12}		1000	2.29×10^{-12}	
1200	4.22×10^{-12}		1200	4.89×10^{-12}	
1300	5.54×10^{-12}		1300	6.73×10^{-12}	
1400	7.08×10^{-12}		1400	8.99×10^{-12}	
1500	8.87×10^{-12}		1500	1.17×10^{-11}	

[a] From Ref. [8]
[b] From Ref. [6]
[c] From Ref. [7]

Table 5 Reaction activation energies E_a (kcal mol^{-1}) for the title reactions

	$CH_2FCHF_2 + OH$		$CHF_2CHF_2 + OH$		$CF_3CHF_2 + OH$	
T range (K)	278 – 323	293 – 441	294 – 434	298 – 358	294 – 441	220 – 360
BMC-CCSD	2.44	2.86	3.76	3.59	4.34	4.35
Exptl.	3.06 ± 1.0[a]	1.98 ± 0.2[b]	3.58 ± 0.3[b]	3.34[c]	2.18 ± 0.2[b]	3.38 ± 0.2[d]

[a] From Ref. [5]
[b] From Ref. [6]
[c] From Ref. [8]
[d] From Ref. [9]

state theory (VTST) at the BMC-CCSD//MPWB1K level over a wide temperature range of 220–1,500 K. The calculated results show that the reactivity decreases with increasing fluorine substitution at the CH_2F group position of fluoroethane, and the order of rate constants is $k_1 > k_2 > k_3$. Theoretical rate constants are in good agreement with the available experimental values. The three parameter expressions (in cm^3 molecule^{-1} s^{-1}) for three reactions within 220–1,500 K are $k_1 = 1.61 \times 10^{-22}\, T^{3.31} \exp(215.6/T)$, $k_2 = 3.27 \times 10^{-21}\, T^{3.05} \exp(747.3/T)$, and $k_3 = 3.21 \times 10^{-22}\, T^{3.42} \exp(955.8/\mathrm{T})$, respectively.

Acknowledgments We thank Professor Donald G. Truhlar for providing of the POLYRATE 9.1 program. This work was supported by the National Natural Science Foundation of China (20333050, 20303007, and 20073014), Doctor Foundation by the Ministry of Education, Foundation for University Key Teacher by the Ministry of Education, the Key Subject of Science and Technology by the Ministry of Education of China, and Key subject of Science and Technology by Jilin Province.

References

1. Tuck R, Plumb A, Condon E (1990) Geophys Rev Lett 17:313
2. Kerr JB (1991) Geophys Rev 96:20703
3. Stolarski R, Bojkoy R, Bishop L, Zerefos C, Staehelin J, Zawodny (1991) J Sci 256:342
4. Kerr RA (1993) Science 262:501
5. Barry J, Sidebottom H (1995) Int J Chem Kinetics 27:27
6. Clyne MAA, Holt PM (1979) J Chem Soc Farad Trans 2, 75, 582
7. Martin JP, Paraskevopoulos G (1983) Can J Chem 61:861
8. Demore WB (1993) Geophys Res 20:1359
9. Talukdar R, Mellouki A, Gierczak T, Burkholder JB, Mckeen SA, Ravishankara AR (1991) J Phys Chem 95:5815
10. Martell JM, Boyd RJ (1995) J Phys Chem 99:13402
11. Hu WP, Truhlar DG (1996) J Am Chem Soc 118:860
12. Truhlar DG (1995) The reaction path in chemistry: current approaches and perspectives. Heidrich D (ed) Kluwer, Dordrecht, p 229
13. Truhlar DG, Garrett BC, Klippenstein SJ (1996) J Phys Chem 100:12771
14. Truhlar DG, Garrett BC (1980) Acc Chem Res 13:440
15. Truhlar DG, Isaacson AD, Garrett BC (1985) The theory of chemical reaction dynamics. Baer M (ed) CRC, Boca Raton, p 65

16. Truhlar DG, Garrett BC (1984) Annu Rev Phys Chem 35:159
17. Frisch MJ, Truck GW, Schlegel HB, Scuseria GE, Robb MA, Cheeseman JR, Zakrzewski VG, Montgomery JA, Stratmann RE, Jr. Burant JC, Dapprich S, Millam JM, Daniels AD, Kudin KN, Strain MC, Farkas O, Tomasi J, Barone V, Cossi M, Cammi R, Mennucci B, Pomelli C, Adamo C, Clifford S, Ochterski J, Petersson GA, Ayala PY, Cui Q, Morokuma K, Malick DK, Rabuck AD, Raghavachari K, Foresman JB, Cioslowski J, Ortiz JV, Boboul AG, Stefnov BB, Liu G, Liaschenko A, Piskorz P, Komaromi L, Gomperts R, Martin RL, Fox DJ, Keith T, Al–Laham MA, Peng CY, Nanayakkara A, Gonzalez C, Challacombe M, Gill PMW, Johnson B, Chen W, Wong MW, Andres JL, Gonzalez C, Head–Gordon M, Replogle ES, Pople JA (2003) GAUSSIAN 03, Revision A.1, Guassian, Pittsburgh
18. Lynch BJ, Zhao Y, Truhlar DG (2005) J Phys Chem A 109:1643
19. Chuang YY, Corchado JC, Truhlar DG (1999) J Phys Chem 103:1140
20. Corchado JC, Chang Y-Y, Fast PL, Villa J, Hu W-P, Liu Y-P, Lynch GC, Nguyen KA, Jackels CF, Melissas VS, Lynch BJ, Rossi I, Coitino EL, Fernandez-Ramos A, Pu J-Z, Albu TV, Steckler R, Garrett BC, Isaacson AD, Truhlar DG (2002) POLYRATE version 9.1, University of Minnesota, Minneapolis
21. Garrett BC, Truhlar DG (1979) J Chem Phys 70:1593
22. Liu Y-P, Lynch GC, Truong TN, Lu D-h, Truhlar DG, Garrett BC (1993) J Am Chem Soc 115:2408
23. Lu DH, Truong TN, Melissas VS, Lynch GC, liu YP, Grarrett BC, Steckler R, Issacson AD, Rai SN, Hancock GC, Lauderdale JG, Joseph T, Truhlar DG (1992) Comput Phys Commun 71:235
24. Beagley B, Brown DE (1979) J Mol Struct 54:175
25. Brown DE, Beagley B (1977) J Mol Struct 38:167
26. Beagley B, Jones MO, Yavari P (1981) J Mol Struct 71:203
27. Hammond GS (1955) J Am Chem Soc 77:334
28. Kalasinsky VF, Anjaria HV, Little TS (1982) J Phys Chem 86:1351
29. Nielsen JR, Richards CM, McMurry HL (1948) J Chem Phys 16:67
30. DeMore WB, Sander SP, Golden DM, Hampson RF, Kurylo MJ, Howard CJ, Ravishankara AR, Kolb CE, Molina MJ (1997) Chemical kinetics and photochemical data for use in stratospheric modelling, JPL Publ. 97–4
31. Lazarou YG (1999) Papagiannakopoulos P Chem Phys Lett 301:19
32. Lide DR (1999) CRC Handbook of chemistry and physics, 80th ed., CRC, New York
33. Ruscic B, Wagner AF, Harding LB, Asher RL, Feller D, Dixon DA, Peterson DA, Song Y, Qian X, Ng CY, Liu JB, Chen WW, Schwenke DW (2002) J Phys Chem A 106:2727
34. Taghikhani M, Parsafar GA (2005) J Phys Chem A 109:8518